ACS APPLIED MATERIALS & INTERFACES

Research Article

www.acsami.org

Carbon-Confined SnO_2-Electrodeposited Porous Carbon Nanofiber Composite as High-Capacity Sodium-Ion Battery Anode Material

Mahmut Dirican,[†,‡] Yao Lu,[†] Yeqian Ge,[†] Ozkan Yildiz,[†] and Xiangwu Zhang*[,†]

[†]Fiber and Polymer Science Program, Department of Textile Engineering, Chemistry and Science, North Carolina State University, Raleigh, North Carolina 27695-8301, United States

[‡]Nano-Science and Nano-Engineering Program, Graduate School of Science, Engineering and Technology, Istanbul Technical University, Istanbul 34469, Turkey

ABSTRACT: Sodium resources are inexpensive and abundant, and hence, sodium-ion batteries are promising alternative to lithium-ion batteries. However, lower energy density and poor cycling stability of current sodium-ion batteries prevent their practical implementation for future smart power grid and stationary storage applications. Tin oxides (SnO_2) can be potentially used as a high-capacity anode material for future sodium-ion batteries, and they have the advantages of high sodium storage capacity, high abundance, and low toxicity. However, SnO_2-based anodes still cannot be used in practical sodium-ion batteries because they experience large volume changes during repetitive charge and discharge cycles. Such large volume changes lead to severe pulverization of the active material and loss of electrical contact between the SnO_2 and carbon conductor, which in turn result in rapid capacity loss during cycling. Here, we introduce a new amorphous carbon-coated SnO_2-electrodeposited porous carbon nanofiber (PCNF@SnO_2@C) composite that not only has high sodium storage capability, but also maintains its structural integrity while ongoing repetitive cycles. Electrochemical results revealed that this SnO_2-containing nanofiber composite anode had excellent electrochemical performance including high-capacity (374 mAh g^{-1}), good capacity retention (82.7%), and large Coulombic efficiency (98.9% after 100th cycle).

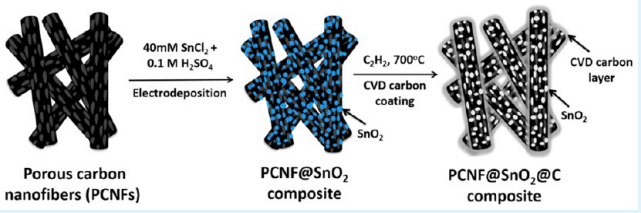

KEYWORDS: *battery, sodium, SnO_2, porous nanofiber, amorphous carbon, capacity*

1. INTRODUCTION

Electrochemical energy storage is currently the most preferred technology for many applications including portable electronic devices, electric cars, and grid storage.[1,2] Among various electrochemical energy storage devices, rechargeable lithium-ion batteries are the most utilized battery technology owning to their distinguished features, such as high energy density, excellent cycling stability and good power performance.[3,4] However, lithium-ion batteries suffer from the ever growing cost of lithium due to limited reserves of lithium element in the earth crust, and hence they are not suitable for large-scale applications, e.g., smart power grids and stationary energy storage.[5,6] Recently, ambient temperature sodium-ion batteries start to gain attention as a promising alternative to lithium-ion batteries mainly because of the high abundance and low cost of sodium resources.[7,8] However, current sodium-ion batteries face the challenges of low energy density and inadequate cycling stability, and they still cannot be used in practical applications. As a result, it is critically important to develop new sodium-ion battery materials with increased capacity and improved cycling stability for smart electric grids and stationary energy storage that will potentially use sodium-ion batteries as the power source.[9−11]

Because the radius of Na ions (~1.09 Å) is much higher than that of Li ions (~0.74 Å), it is crucial to choose a convenient anode material with sufficient Na-insertion capacity and cycling capability.[12,13] Graphite is the most used anode material in commercial lithium-ion batteries, but its layered structure can only store few sodium ions.[14] On the other hand, hard carbons have disordered structure and large interlayer distance, and hence they have been demonstrated as suitable anode material for Na storage.[15] Recently, transition metals (e.g., tin, antimony, and germanium) and their oxides have been found to be promising anode material candidates for sodium-ion batteries because they exhibit high capacities through intercalating large amount of Na ions based on the conversion mechanism.[16,17] However, despite their high sodium storage capability, the large volume change upon sodium insertion into these anodes leads to severe pulverization of active material and hence detrimentally damaged electrode structure.[13,18] As a result, anodes based on transition metals and their oxides often experience intense capacity loss during repeated charging and discharging. Currently, using the nanoscaled active materials and combining them with carbon structures are two most-studied approaches for alleviating the volume expansion problem.[18,19]

Because of their distinguished features including high capacity, low toxicity, and high availability, tin oxides (SnO_x,

Received: May 19, 2015
Accepted: August 7, 2015
Published: August 7, 2015

DOI: 10.1021/acsami.5b04338
ACS Appl. Mater. Interfaces 2015, 7, 18387−18396

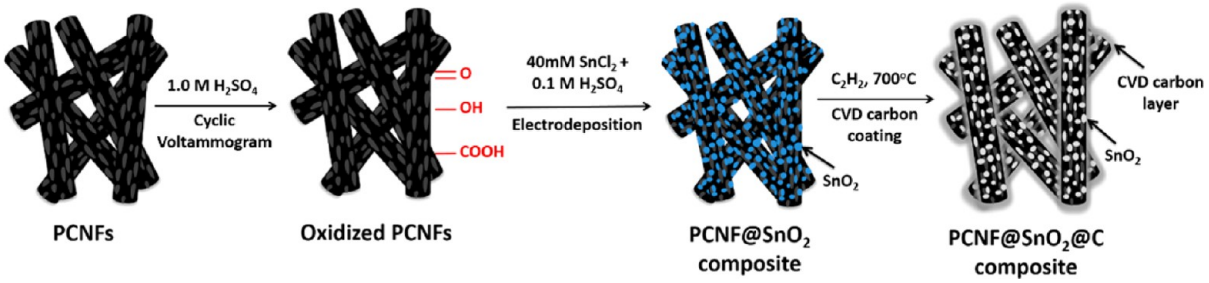

Figure 1. Schematic of the fabrication procedures of PCNF@SnO_2 and PCNF@SnO_2@C composites.

x = 1 and 2) are a promising anode material candidate for future sodium-ion batteries. Electrochemical reduction reaction of SnO_2 in a Na-ion battery can be expressed using the following equation, based on the Na−Sn binary phase diagram:

$$SnO_2 + 4Na^+ + 4e^- \rightarrow Sn + 2Na_2O \quad (1)$$

In accordance with this reaction, the theoretical capacity of SnO_2 is calculated to be 667 mAh g^{-1}.[20] Recently, SnO_2 nanoparticle-loaded graphene and carbon nanotube composite materials have been studied as high-capacity sodium-ion battery anode materials. For instance, Wang et al. introduced a SnO_2 nanoparticle-added reduced graphene oxide nanocomposite anode for sodium-ion batteries and reported a reversible capacity of 330 mAh g^{-1} at 100 mA g^{-1} for 150 cycles.[21] Su and his team prepared SnO_2@graphene nanocomposites and obtained a reversible capacity of 569 mAh g^{-1} after 100 cycles at 40 mA g^{-1}.[22] Wang et al. loaded SnO_2 nanocrystal onto multiwalled carbon nanotube and achieved a reversible capacity of 400 mAh g^{-1} after 50 cycles at 50 mA g^{-1}.[20] It is therefore believed that in a typical nanostructured SnO_2/carbon based composite anode, the carbon matrix accommodates the volume expansion of the active SnO_2 material during charge and discharge processes by serving as a physical buffer, that is, the cushion effect. High-capacity anodes composed of SnO_2 nanoparticle-electrodeposited electrospun carbon nanofiber (CNF) composites have been previously reported for lithium-ion batteries.[23,24] Similar structure can be used in sodium-ion batteries as well. One of the easy methods for integration of SnO_2 with CNFs is the electrodeposition of SnO_2 nanoparticles directly onto electrospun CNFs.[24,25] Electrodeposition is one of the most effective methods for modifying the structural features of carbon nanomaterials and it enables the formation and growth of metal oxide clusters on the surfaces of one-dimensional carbon materials.[26,27] In contrast to many other coating methods, e.g., chemical vapor deposition, physical vapor deposition, atomic layer deposition, etc., the electrodeposition technique is considerably inexpensive and scalable, and hence has been used as an effective low-temperature processing approach.[25]

In this study, electrodeposited SnO_2/porous carbon nanofiber (PCNF@SnO_2) and chemical vapor deposition (CVD) carbon-confined electrodeposited SnO_2/porous carbon nanofiber (PCNF@SnO_2@C) composites were introduced as sodium-ion battery anode materials. The PCNF structure was used to enhance the surface area of nanofibers for achieving the high loading amount of electrodeposited SnO_2 nanoparticles. The fabrication processes of PCNF@SnO_2 and PCNF@SnO_2@C) composites are schematically represented in Figure 1. Prior to electrodeposition, electrospun PCNFs were oxidized in an acidic solution to form surface functional groups and create defect sites for easier particle attachment. After surface oxidation, electrodeposition of SnO_2 nanoparticles was conducted on the oxidized PCNFs to produce the PCNF@SnO_2 composite. To achieve further improvement on the anode performance, nanoscale carbon postcoating of the PCNF@SnO_2 composite was performed by the CVD method, and carbon-confined PCNF@SnO_2 (PCNF@SnO_2@C) composite was obtained. Electrochemical performance studies revealed that the as-prepared PCNF@SnO_2@C composite anode possessed excellent electrochemical performance including high-capacity (374 mAh g^{-1}), good capacity retention (82.7%), and large Coulombic efficiency (98.9% after 100th cycle).

2. EXPERIMENTAL SECTION

2.1. Electrospinning and Carbonization of Porous Carbon Nanofibers. A DMF (Aldrich) solution of 8 wt % PAN (150 000 g mol^{-1}, Pfaltz & Bauer Inc.)/PMMA (Aldrich) blend was prepared with a PAN-to-PMMA mass ratio of 9/1 at 60 °C and it was mechanically stirred for 24 h. The as-prepared PAN/PMMA blend solution was then electrospun into nanofibers under a flow rate of 0.75 mL/h at 16 kV with tip-to-collector distance of 20 cm. Electrospun PAN/PMMA nanofibers were stabilized in air at 280 °C for 5.5 h (heating rate = 5 °C min^{-1}) and carbonized at 700 °C in argon for 2 h (heating rate = 2 °C min^{-1}). During the thermal treatment, PAN was pyrolyzed to carbon while PMMA was decomposed to generate a porous structure in the carbon matrix. Carbonization temperature and time used in this study were determined based on our previously reported study, in which different carbonization conditions were examined to obtain appropriate nanofiber structure for optimum electrochemical performance.[28] The resultant PCNFs were used as the working electrode in the electrodeposition of SnO_2 nanoparticles.

2.2. Electrodeposition and CVD Coating of Porous Carbon Nanofibers. Electrodeposition process was performed by using a three-electrode cell consisting of a working electrode (PCNFs), a counter electrode (Pt wire), and a reference electrode (Ag/AgCl/4.0 M KCl). Before electrodeposition, PCNFs were oxidized in a 1 M sulfuric acid (H_2SO_4, Aldrich) solution using the cyclic voltammetry method on a Reference 600 Potentiostat/Galvanostat/ZRA (GAMRY) electrochemical workstation between −0.7 and 1.2 V with a scan rate of 50 mV s^{-1} for 100 cycles. Electrodeposition of SnO_2 nanoparticles on PCNFs was conducted in a 0.04 M tin(II) chloride ($SnCl_2$, Aldrich) + 0.1 M H_2SO_4 solution at room temperature by applying a potential of −0.2 V vs Ag/AgCl/4.0 M KCl for 20 h using the same instrument. Our previously reported study revealed that an electrodeposition time of 20 h gave the maximum SnO_2 loading onto electrospun CNFs.[25] The SnO_2-electrodeposited nanofibers were then annealed at 700 °C for 1 h in argon to form the PCNF@SnO_2 composite. To ensure the reproducibility of the process, electrodeposition experiments were performed at least three times on each sample.

The as-prepared PCNF@SnO_2 composite mat was placed on a quartz substrate located in a horizontal CVD tube furnace (inner tube diameter: around 6.8 cm) to carry out the CVD carbon coating by using acetylene (C_2H_2) as the carbon precursor gas. The PCNF@

DOI: 10.1021/acsami.5b04338
ACS Appl. Mater. Interfaces 2015, 7, 18387−18396

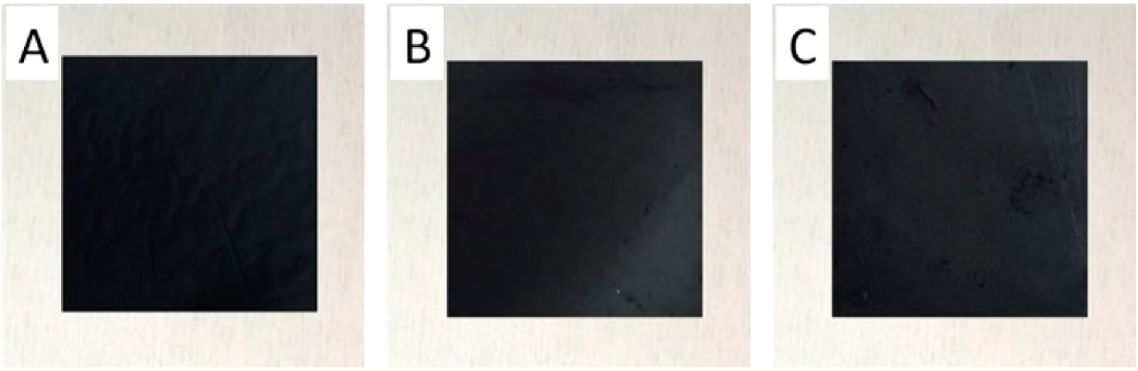

Figure 2. Photographs of (A) PCNFs, (B) PCNF@SnO_2 composite, and (C) PCNF@SnO_2@C composite.

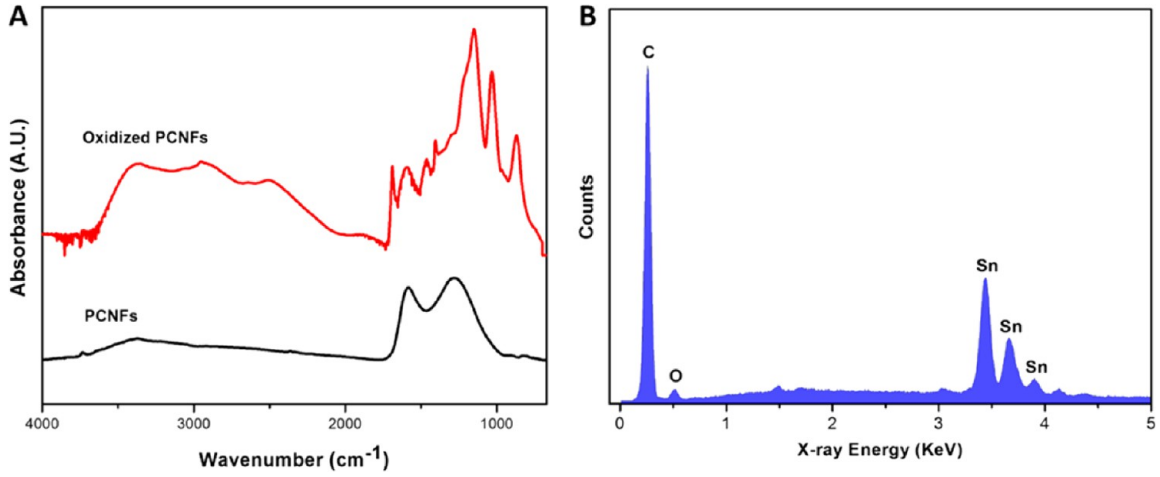

Figure 3. FTIR spectra of PCNFs and oxidized PCNFs (A) and EDS spectrum of PCNF@SnO_2@C composite (B).

SnO_2@C composite was obtained by conducting the CVD carbon coating process at 700 °C for 1 h with 600 sccm flow rate of acetylene while the system was set 20 Torr. These processing conditions ensured the uniform deposition of thin carbon layer on the high-surface area PCNF@SnO_2 mat. Our previous work also showed that these CVD processing conditions produced the most uniform amorphous carbon coating.[29]

2.3. Structure Characterization. The surface morphology of nanofiber composites was investigated using an field emission scanning electron microscope (FE-SEM, FEI Verios 460 L) and a scanning transmission electron microscope (STEM, JEOL 2000FX). The chemical and crystallographic structures of nanofiber composites were examined by using Fourier transform infrared spectroscopy (FTIR, Nicolet Nexus 470) and wide-angle X-ray diffraction (WAXD, Rigaku Smartlab). The elemental compositions of nanofiber composites were studied by elemental analysis (PerkinElmer 2400 Series II CHNS/O Elemental Analyzer).

2.4. Electrochemical Evaluation. The electrochemical properties of nanofiber composites were tested using CR 2032-type coin cells. The working electrodes were prepared by mixing 80% active material, 12% carbon black, and 8% sodium-alginate binder dissolved in deionized water. The slurry was coated onto a copper foil as current collector and dried at 80 °C for 12 h. The average mass loading of the electrodes used in this study was 0.95 mg cm^{-2}. Electrodes were punched into circular disks with 0.5 in. in diameter. Pure sodium metal (Aldrich) was used as the counter electrode. The electrolyte used was 1 M sodium perchlorate ($NaClO_4$) dissolved in ethylene carbonate (EC) and dimethyl carbonate (DMC) (1:1 in volume). Glass fiber mat (Whatman) was used as the separator. Coin cells were assembled in a high-purity argon-filled glovebox. Cyclic voltammetry (CV) tests were conducted using Reference 600 Potentiostat/Galvanostat/ZRA (GAMRY). Galvanostatic charge−discharge experiments were carried out at constant current density of 50 mA g^{-1} using a LAND-CT 2001A battery test system. All cells were tested with cutoff potentials of 0.01 and 3.00 V. The rate capabilities of nanofiber composites were evaluated at current densities of 50, 100, 200, 400, and 800 mA g^{-1} by using the same instrument.

The reproducibility of the electrochemical performance tests was ensured by performing all experimental measurements on at least ten samples for each nanofiber composite.

3. RESULTS AND DISCUSSION

3.1. Morphology and Structure. As demonstrated in Figure 1, before the electrodeposition process an oxidation treatment of PCNFs was conducted with 1 M of H_2SO_4 solution to generate negatively charged functional groups such as quinoid (=O), carboxyl (−COOH), and hydroxyl (−OH) on the nanofiber surfaces. These functional groups were utilized during electrodeposition to provide defect sites for the attachment of SnO_2 nanoparticles.[30] Following the oxidation treatment, SnO_2 nanoparticles were electrodeposited onto the surfaces of PCNFs, during which the SO_4^{2-} ions in the

Table 1. Compositions of PCNF@SnO_2 and PCNF@SnO_2@C Composites Based on Element Analysis Measurement

description of nanofiber composites	compositions of nanofiber composites (wt %)	
	C	SnO_2
PCNF@SnO_2 composite	47.6	40.8
PCNF@SnO_2@C composite	50.6	38.5

DOI: 10.1021/acsami.5b04338
ACS Appl. Mater. Interfaces 2015, 7, 18387−18396

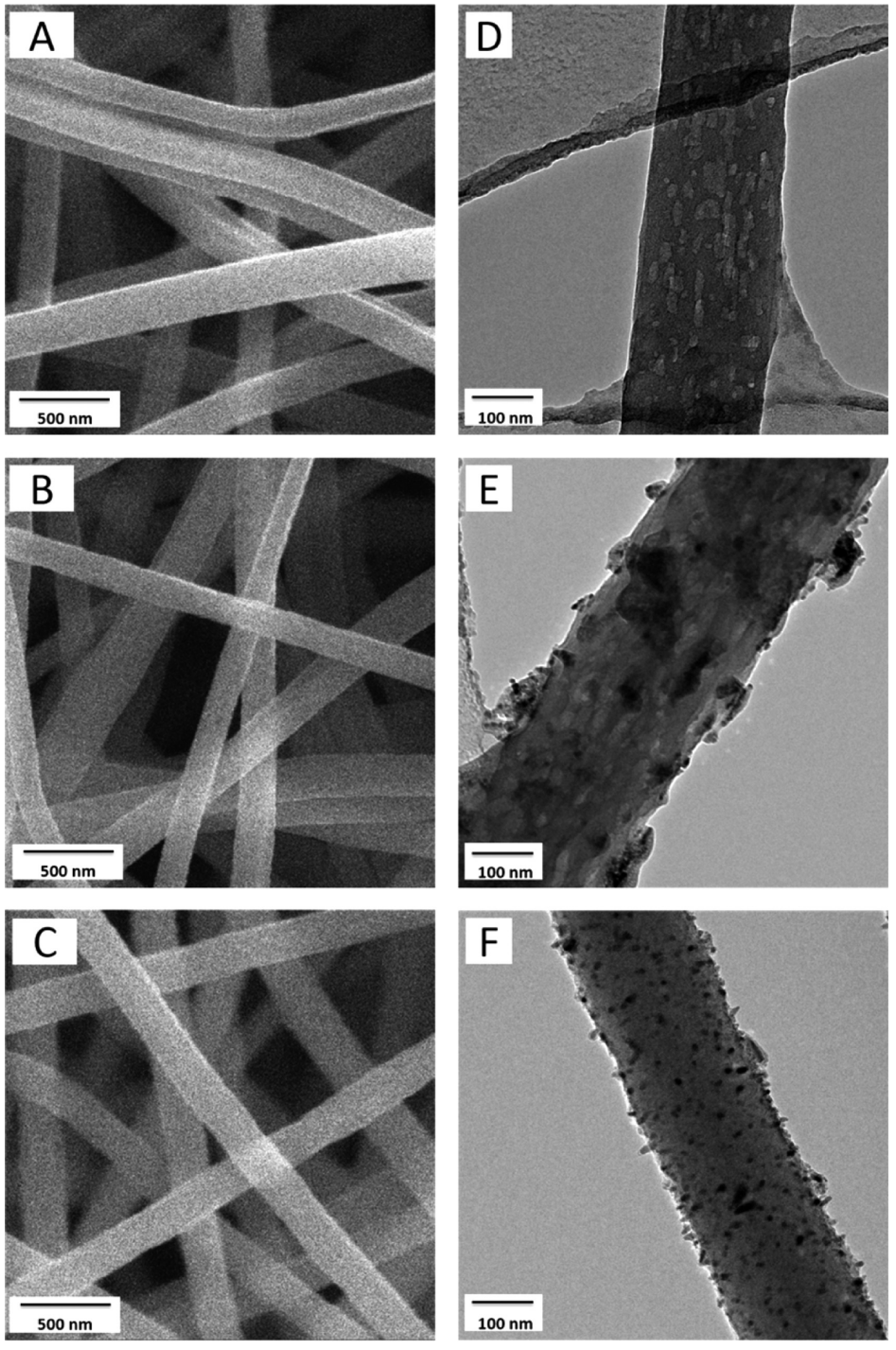

Figure 4. SEM images of (A) PCNFs, (B) PCNF@SnO_2 composite, and (C) PCNF@SnO_2@C composite, and TEM images of (D) PCNFs, (E) PCNF@SnO_2 composite, and (F) PCNF@SnO_2@C composite.

acidic electrodeposition solution were electrochemically reduced on PCNF surfaces, accompanied by OH^- ion formation in the solution. The deposition of SnO_2 nanoparticles was the direct result of the subsequent reaction of tin(II) with OH^- ions on the nanofiber surfaces. The as-prepared PCNF@SnO_2 composite was then coated with amorphous carbon layers through the CVD method. Photographs of as-prepared PCNFs, PCNF@SnO_2 composite, and PCNF@SnO_2@C composite are shown in Figure 2. It was found that the physical appearances of all three different samples were the same. The electrodeposited SnO_2 nanoparticles and CVD carbon coating were not visible from these optical images.

FTIR spectra of PCNFs and oxidized PCNFs are shown in Figure 3A. The chemical functional groups formed on fiber surfaces during the oxidation process were verified by the FTIR results. As shown in Figure 3A, two characteristic peaks were found for unoxidized PCNFs at 1280 and 1590 cm^{-1}, corresponding to the C−C and C═C stretch bonds, respectively. In the case of oxidized PCNFs, two broad peaks were observed at 3333 and 2957 cm^{-1}, which were ascribed to the −OH vibration of the −COOH group. An intense peak was

DOI: 10.1021/acsami.5b04338
ACS Appl. Mater. Interfaces 2015, 7, 18387−18396

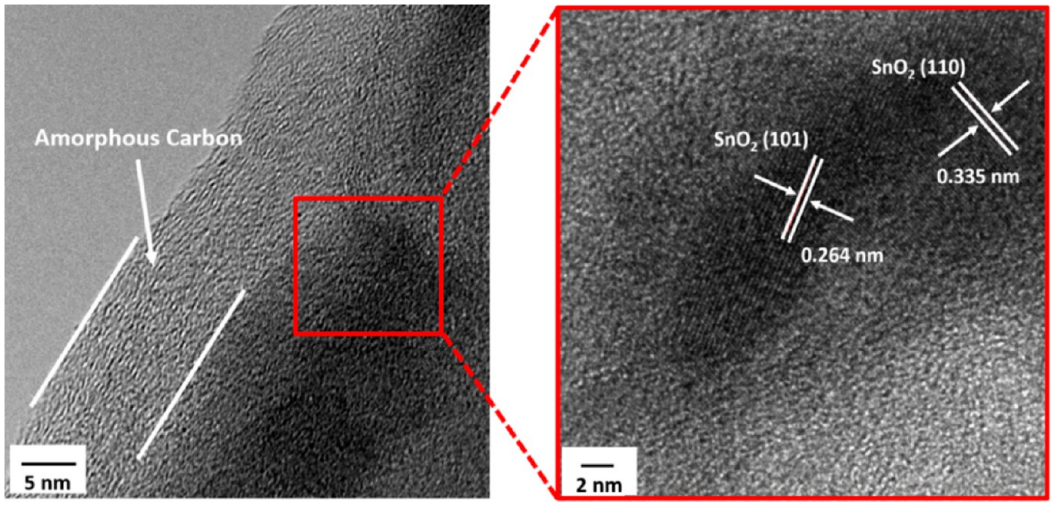

Figure 5. High-magnification TEM images of PCNF@SnO_2@C composite.

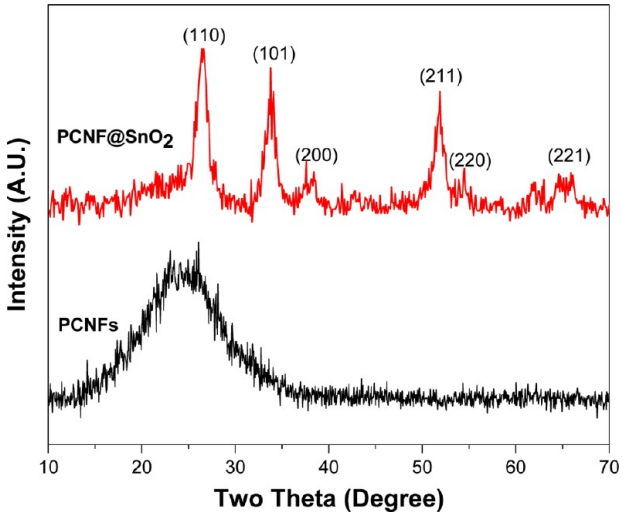

Figure 6. WAXD patterns of PCNFs and PCNF@SnO_2 composite.

also found at 1162 cm^{-1}, corresponding to the −C−O stretching of the − C−OH group. In addition, oxidized PCNFs also showed two characteristic bending mode peaks at 1733 and 1690 cm^{-1}, respectively, which were attributed to the − C═O stretch bonds in esters and benzophenones.[31]

Figure 3B shows the energy-dispersive X-ray spectroscopy (EDS) analysis spectrum of the PCNF@SnO_2@C composite. The EDS result verified the presence of tin, oxygen, and carbon. The SnO_2 contents in PCNF@SnO_2 and PCNF@SnO_2@C composites were evaluated by the elemental analysis (Table 1). During the elemental analysis, the SnO_2 contents were calculated based on the carbon, hydrogen and nitrogen compositions by neglecting other impurities. It was observed that SnO_2 contents were 40.8% and 38.5%, respectively, in PCNF@SnO_2 and PCNF@SnO_2@C composites. Elemental analysis results also demonstrated that after CVD carbon coating, the total carbon amount in the composites increased simply due to the introduction of carbon coating layers on the fiber surfaces.

Figure 4A−C compare SEM images of PCNFs, PCNF@SnO_2, and PCNF@SnO_2@C composites. From Figure 4, it is observed that all three nanofiber samples have comparable fibrous morphology. SEM image of the PCNF@SnO_2 composite revealed that uniform electrodeposition of SnO_2 nanoparticles throughout the nanofiber surfaces was achieved without the formation noticeable agglomerations. Due to the limited resolution of SEM, the porous nature of the nanofibers and the nanoscale carbon coating layers on PCNF@SnO_2@C composites could not be observed in the SEM images. Therefore, TEM experiments were performed to show the porous structure of the nanofibers and the nanoscale CVD carbon coating layers, as discussed below.

TEM images of PCNFs, PCNF@SnO_2, and PCNF@SnO_2@C were presented in Figure 4D−F, respectively. The porous nature of PCNFs, formed by the decomposition of PMMA, was seen in the TEM image (Figure 4D). As shown in Figure 4E, after the electrodeposition, SnO_2 nanoclusters were deposited along the nanofiber surfaces, that is, forming the PCNF@SnO_2 composite. The CVD amorphous carbon coating, which was comparatively darker than the SnO_2 deposition, was also observed on the PCNF@SnO_2@C composite (Figure 4F). High-magnification TEM images of PCNF@SnO_2@C composite are shown in Figure 5 to further illustrate the carbon and SnO_2 structures. It was observed that the surface of the PCNF@SnO_2@C composite had an amorphous carbon layer of around 10 nm thick. This carbon coating layer is crucially important for stable SEI formation on the active material surface during the first few charge and discharge cycles. As shown in Figure 5, two different lattice fringes were present with the lattice spacings of around 0.335 and 0.264 nm, respectively, and they were attributed to the (110) and (101) planes of SnO_2 nanoparticles.

The X-ray diffraction (XRD) patterns of PCNFs and PCNF@SnO_2, which were annealed at 700 °C for 1 h in argon atmosphere, are shown in Figure 6. For PCNF@SnO_2 composite, diffraction peaks at 2θ of about 27°, 34°, and 52° were indexed as the (110), (101), and (211) planes of the tetragonal SnO_2 phase (JCPDS No. 41-1445), respectively.[32,33] In addition, as shown in Figure 6, both PCNF and PCNF@SnO_2 composites exhibited a broad, but weak diffraction peak at around 2θ = 25°, which was indexed as the (002) planes of disordered carbon, revealing the amorphous nature of the carbon nanofiber matrix.[29,34]

3.2. Electrochemical Performance. Cyclic voltammetry (CV) and galvanostatic charge−discharge tests were performed to evaluate the electrochemical properties of the nanofiber

DOI: 10.1021/acsami.5b04338
ACS Appl. Mater. Interfaces 2015, 7, 18387−18396

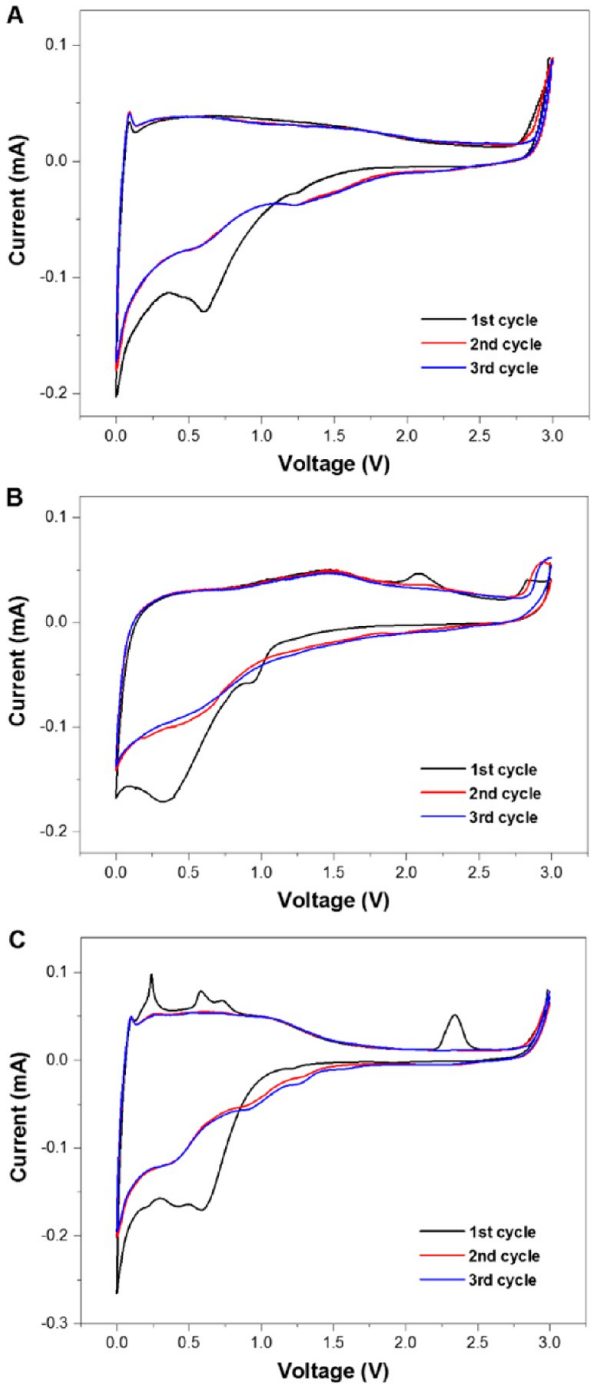

Figure 7. Cyclic voltammetry curves of (A) PCNFs, (B) PCNF@SnO_2 composite, and (C) PCNF@SnO_2@C composite.

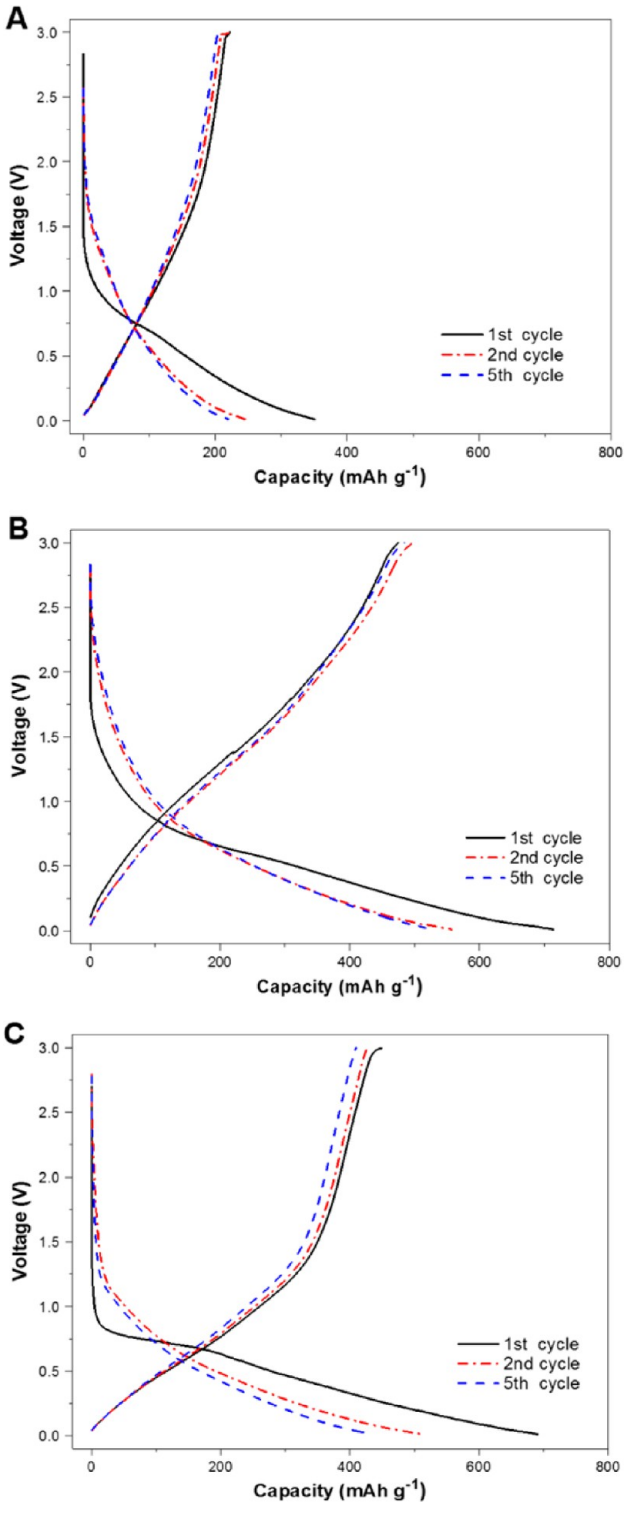

Figure 8. Galvanostatic charge−discharge profiles of (A) PCNFs, (B) PCNF@SnO_2 composite, and (C) PCNF@SnO_2@C composite.

composites for use as sodium-ion battery anode materials. CV measurements were conducted on PCNFs, PCNF@SnO_2, and PCNF@SnO_2@C with a scan rate of 0.1 mV s^{-1} between 0 and 3 V to reveal the redox reactions and the results are shown in Figure 7. For the PCNFs, three-cathodic peaks were observed at around 1.28, 0.68, and 0 V during the first scan (Figure 7A). The first peak at 1.28 V was ascribed to the reaction of sodium ions on the carbon nanofiber surface.[35] The irreversible peak at 0.68 V was attributed to the decomposition of sodium electrolyte and subsequent solid electrolyte interphase (SEI) formation.[14] A third cathodic peak was observed at around 0 V, indicating the insertion of sodium ions into the porous carbon matrix.[36] In the anodic scan of the PCNFs, a small peak indexed at around 0.2 V in the first and subsequent cycles was attributed to the extraction of sodium ions from porous carbon.[35] From the CV curve of the PCNF@SnO_2 composite, reduction peaks ranging from 0.85 to 0.25 V observed during the first cathodic scan were associated with the irreversible decomposition of the electrolyte to form SEI films and the irreversible reactions between sodium ions and SnO_2 to form Na_xSn alloys (Figure

DOI: 10.1021/acsami.5b04338
ACS Appl. Mater. Interfaces 2015, 7, 18387−18396

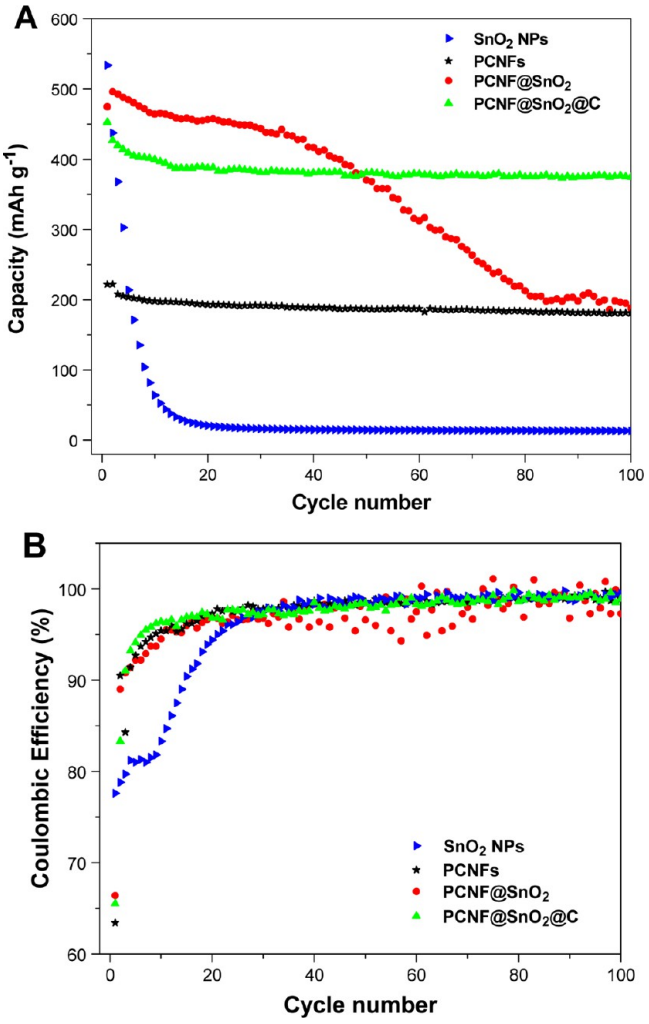

Figure 9. Cycling performance (A) and Coulombic efficiencies (B) of SnO_2 nanoparticles, PCNFs, PCNF@SnO_2 composite, and PCNF@SnO_2@C composite.

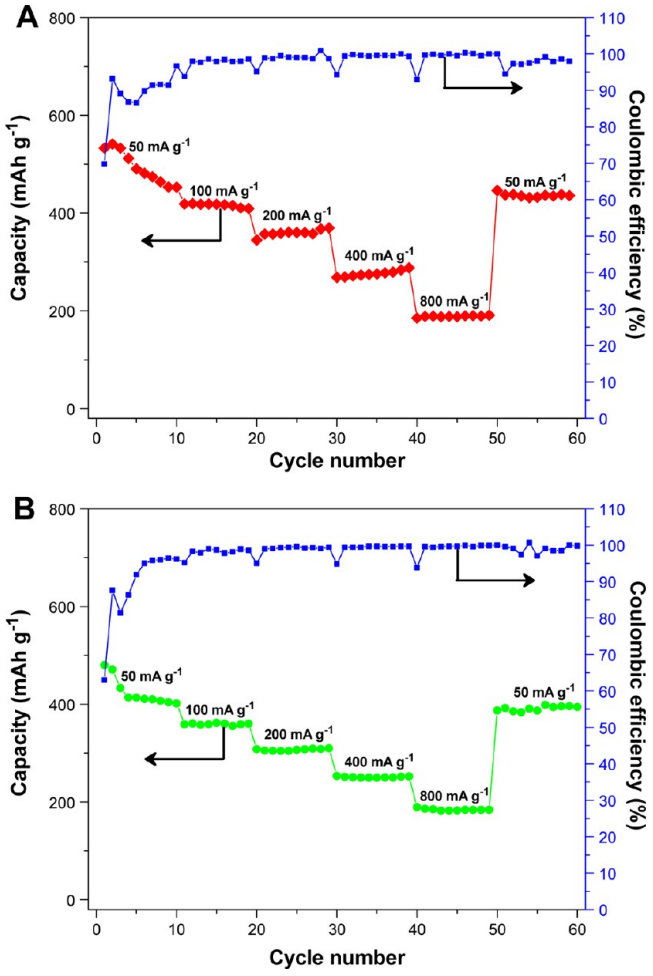

Figure 10. Rate capabilities of (A) PCNF@SnO_2 composite and (B) PCNF@SnO_2@C composite cycled at different current densities.

7B). The peaks in the anodic scan were ascribed to the reversible dealloying of Na_xSn.[37] The CV curves in the subsequent cycles were similar, indicating that the electrochemical reactions in the PCNF@SnO_2 composite are highly reversible. In the first cathodic scan of the PCNF@SnO_2@C composite, peaks ranging from 0.8 to 0.2 V were ascribed to the irreversible decomposition of the electrolyte and the reaction of SnO_2 and sodium ions to form Na_xSn alloys (Figure 7C). Oxidation peaks in the anodic scan were associated with the reversible dealloying of Na_xSn.[20] After the first scan, the intensities of redox peaks decreased, indicating the loss of irreversible capacity that could be attributed to the formation of SEI film in the initial cycle. However, the CV curves in the subsequent cycles did not show apparent changes, demonstrating the excellent electrochemical reversibility of the PCNF@SnO_2@C composite.

To investigate the electrochemical performance of the nanofiber composites, galvanostatic charge−discharge tests were performed at a constant current density of 50 mA g^{-1} between 0.01 and 3.0 V. The charge−discharge curves for the first, second and fifth cycles of PCNFs, PCNF@SnO_2, and PCNF@SnO_2@C are shown in Figure 8. It is seen that both PCNF@SnO_2 and PCNF@SnO_2@C composites exhibited higher initial sodium storage capability than PCNFs. At the first cycle, the discharge capacities were 350, 715, and 691 mAh g^{-1}, respectively, for PCNFs, PCNF@SnO_2, and PCNF@SnO_2@C. The discharge capacities decreased to 245, 557, and 512 mAh g^{-1}, respectively, at the second cycle. In the case of PCNF@SnO_2 and PCNF@SnO_2@C composites, a plateau was also observed at around 0.8 V at the first discharge, corresponding to the reaction between SnO_2 and Na to form nanocrystalline Na_xSn alloys and Na_2O. During the charge, the process was reversed. However, this voltage plateau became larger after the introduction of nanoscale carbon coating layers. The overall reduction reactions could be ascribed as follows:

$$SnO_2 + 4Na^+ + 4e^- \rightarrow Sn + 2Na_2O \quad (2)$$

$$Sn + xNa^+ + xe^- \leftrightarrow Na_xSn \quad (3)$$

The first reaction, that is, the reduction of SnO_2 to Sn, was irreversible.[21,22] Apparent capacity loss was observed during the initial cycles because of the formation of a solid electrolyte interface (SEI) at low voltage in addition to the first reaction. In contrast to the first reaction, the second reaction was reversible. Sodium ions were stored and released by the formation of alloyed Na_xSn and dealloyed Sn, respectively, during sodiation and desodiation processes. First-cycle Coulombic efficiency values of PCNFs, PCNF@SnO_2, and PCNF@SnO_2@C were 63.4%, 66.4%, and 65.1%, respectively. At the fifth cycle, the

DOI: 10.1021/acsami.5b04338
ACS Appl. Mater. Interfaces 2015, 7, 18387−18396

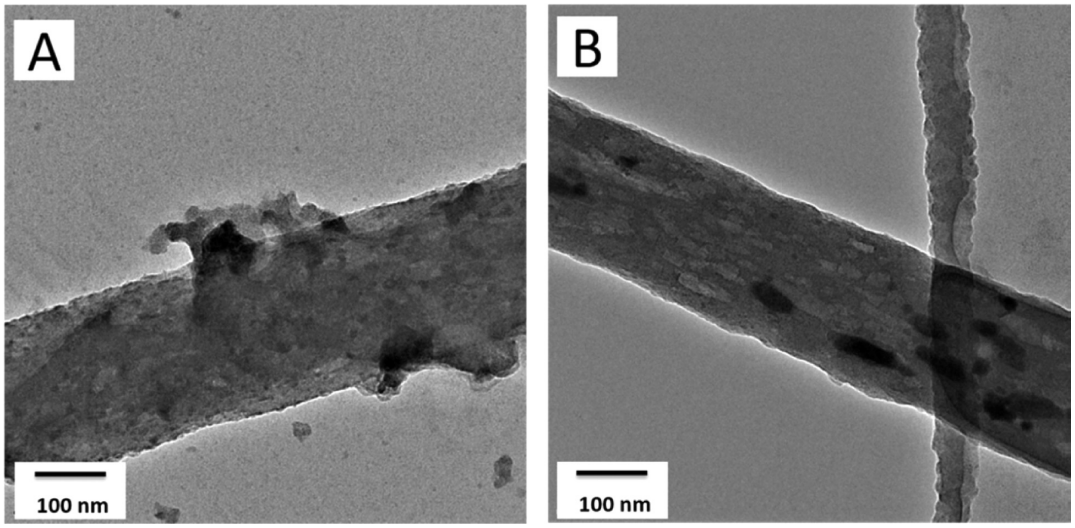

Figure 11. TEM images of cycled (A) PCNF@SnO_2 composite and (B) PCNF@SnO_2@C composite after 100 cycles.

Coulombic efficiency values increased to 92.7%, 92.2%, and 94.1%, respectively.

The cycling performance of PCNFs, PCNF@SnO_2, and PCNF@SnO_2@C was evaluated at a constant current density of 50 mA g^{-1} and results are demonstrated in Figure 9. For comparison, the cycling performance of bare SnO_2 nanoparticles is also shown. At the 100th cycle, the capacity retention and Coulombic efficiency of electrospun PCNFs were around 81.4% and 98.9%, respectively. However, the capacity retention of bare SnO_2 nanoparticles at the 100th cycle was only 2.5%. From Figure 9, it is also seen that the PCNF@SnO_2 composite had a much higher sodium capacity than PCNFs and bare SnO_2 nanoparticles at the initial cycles, but it exhibited faster capacity decay during ongoing cycles. Capacity retention and Coulombic efficiency of PCNF@SnO_2 composite at the 100th cycle were around 39.6% and 97.6%, respectively. On the other hand, the cycling performance of PCNF@SnO_2 composite was considerably enhanced by nanoscale carbon coating. Among all four samples studied, the PCNF@SnO_2@C composite possessed the highest capacity and capacity retention. At the 100th cycle, the PCNF@SnO_2@C composite exhibited a capacity of around 374 mAh g^{-1}, with a corresponding capacity retention of 82.7%. Furthermore, the Coulombic efficiency of the PCNF@SnO_2@C composite was as high as 98.9% at the 100th cycle. In this composite, the porous structure of the carbon nanofiber matrix worked together with the nanoscale carbon coating to help absorb the volume expansion of SnO_2 particles, which led to the improvement in cycling performance. The nanoscale carbon coating layer could also support stable SEI formation on the fiber surface by serving as a barrier to hinder direct contact of the electrolyte with the active SnO_2 material, which in turn resulted in increased Coulombic efficiency. Similar electrode structure was previously reported by Wang et al.[21] They introduced ultrafine SnO_2 nanoparticle loaded reduced graphene oxide nanocomposites as an anode material for sodium-ion batteries, and they achieved a capacity of about 245 mAh g^{-1} at a current density of 100 mA g^{-1} over 150 cycles. Their anode also delivered a capacity retention of 81.3% over 150 cycles. In another study, Wang et al. reported a SnO_2@multiwalled carbon nanotube (MWCNT) nanocomposite, which delivered a reversible capacity of about 400 mAh g^{-1} at a current density of 50 mA g^{-1} over 50 cycles. Furthermore, they reported a capacity retention of 72% over 50 cycles for their SnO_2@MWCNT nanocomposite anode.[20]

The rate capability of PCNF@SnO_2 and PCNF@SnO_2@C composites was investigated under different current densities and results are demonstrated in Figure 10. PCNF@SnO_2 composite delivered average charge capacities of around 493, 416, 359, 276, and 189 mAh g^{-1}, respectively, at 50, 100, 200, 400, and 800 mA g^{-1} (Figure 10A). No apparent change was observed for the Coulombic efficiency as the current density increased. After applying 50 cycles at higher current densities, the charge capacity value increased back to 436 mAh g^{-1} when the current density returned to 50 mAh g^{-1}. On the other hand, PCNF@SnO_2@C composite delivered average capacities of around 425, 359, 307, 251, and 184 mAh g^{-1}, respectively, at 50, 100, 200, 400, and 800 mA g^{-1} (Figure 10B). After ongoing 50 cycles at higher current densities, the capacity of PCNF@SnO_2@C composite increased back to 391 mAh g^{-1} under a reduced current density of 50 mAh g^{-1}. This relatively high capacity (391 mAh g^{-1}), which is similar to those of initial cycles, indicated the good rate capability of PCNF@SnO_2@C composite. Similar to PCNF@SnO_2 composite, no apparent Coulombic efficiency change was observed for PCNF@SnO_2@C composite as the current density increased. This result showed that the CVD carbon coating did not have apparent negative effect on the rate performance and the resultant PCNF@SnO_2@C composite can be potentially used as the anode material in sodium-ion batteries for high rate applications. Since the carbon coating has an amorphous structure, it allowed sodium ions to penetrate through and eventually be inserted into the active SnO_2 material. The penetration of sodium ions through amorphous carbon coating was also observed by Jian and co-workers.[38] They prepared carbon-confined $Na_3V_2(PO_4)_3$ composite, and found that Na ions were able to penetrate through the thin carbon coating layers and reach the encapsulated $Na_3V_2(PO_4)_3$ structure.

To investigate the morphology change of PCNF@SnO_2 and PCNF@SnO_2@C composites after cycling, the tested cells were disassembled and analyzed by using TEM (Figure 11). The cycled electrodes were washed with a HCl solution to remove the formed SEI film prior to TEM characterization. As shown in Figure 11A, because of the repetitive volume

DOI: 10.1021/acsami.5b04338
ACS Appl. Mater. Interfaces 2015, 7, 18387−18396

expansion and contraction of electrodeposited SnO_2 nanoparticles during cycling, the PCNF@SnO_2 composite was subjected to major structural damage and many SnO_2 nanoparticles were pulverized or detached from the carbon matrix. Contrary to the PCNF@SnO_2 composite, most of the SnO_2 nanoparticles in the PCNF@SnO_2@C composite were maintained on the porous carbon nanofibers after cycling, without extreme structural damage to the nanofiber surface (Figures 11B). Therefore, these results demonstrated that CVD amorphous carbon coating helped maintain the structural integrity of the PCNF@SnO_2@C composite during repeated charge−discharge cycling.

4. CONCLUSIONS

PCNF@SnO_2 composite was introduced as sodium-ion battery anode material by the electrodeposition of SnO_2 nanoparticles on porous carbon nanofibers. To improve the cycling performance, CVD carbon coating was applied onto the PCNF@SnO_2 surface. In the resultant PCNF@SnO_2@C composite, the porous structure of carbon nanofiber matrix worked together with nanoscale CVD carbon coating layers to help absorb the volume expansion of SnO_2 particles, which led to significant improvement in cycling stability. Electrochemical test results demonstrated that at the 100th cycle, the PCNF@SnO_2@C composite delivered a capacity of around 374 mAh g^{-1}, which was much higher than that (188 mAh g^{-1}) of the PCNF@SnO_2 composite. At the same time, the capacity retention and Coulombic efficiency of the PCNF@SnO_2@C composite were 82.7% and 98.9%, respectively, even at the 100th cycle.

AUTHOR INFORMATION

Corresponding Author

*Tel: 919-515-6547. Fax: 919-515-6532. E-mail: xiangwu_zhang@ncsu.edu.

Notes

The authors declare no competing financial interest.

ACKNOWLEDGMENTS

The authors thank Dr. Philip D. Bradford and Ozkan Yildiz for use of the chemical vapor deposition furnace.

REFERENCES

(1) Liu, N.; Wu, H.; McDowell, M. T.; Yao, Y.; Wang, C.; Cui, Y. A Yolk-Shell Design for Stabilized and Scalable Li-Ion Battery Alloy Anodes. *Nano Lett.* **2012**, *12*, 3315−21.

(2) Ji, L.; Toprakci, O.; Alcoutlabi, M.; Yao, Y.; Li, Y.; Zhang, S.; Guo, B.; Lin, Z.; Zhang, X. α-Fe_2O_3 Nanoparticle-Loaded Carbon Nanofibers as Stable and High-Capacity Anodes for Rechargeable Lithium-Ion Batteries. *ACS Appl. Mater. Interfaces* **2012**, *4*, 2672−2679.

(3) Yu, X.; Yang, S.; Zhang, B.; Shao, D.; Dong, X.; Fang, Y.; Li, Z.; Wang, H. Controlled Synthesis of SnO_2@Carbon Core-Shell Nanochains as High-Performance Anodes for Lithium-Ion Batteries. *J. Mater. Chem.* **2011**, *21*, 12295−12302.

(4) Dirican, M.; Yanilmaz, M.; Fu, K.; Yildiz, O.; Kizil, H.; Hu, Y.; Zhang, X. Carbon-Confined PVA-Derived Silicon/Silica/Carbon Nanofiber Composites as Anode for Lithium-Ion Batteries. *J. Electrochem. Soc.* **2014**, *161*, A2197−A2203.

(5) Ge, Y.; Jiang, H.; Zhu, J.; Lu, Y.; Chen, C.; Hu, Y.; Qiu, Y.; Zhang, X. High Cyclability of Carbon-Coated TiO_2 Nanoparticles as Anode for Sodium-Ion Batteries. *Electrochim. Acta* **2015**, *157*, 142−148.

(6) Wu, L.; Buchholz, D.; Bresser, D.; Chagas, L. G.; Passerini, S. Anatase TiO_2 Nanoparticles for High Power Sodium-Ion Anodes. *J. Power Sources* **2014**, *251*, 379−385.

(7) Datta, M. K.; Epur, R.; Saha, P.; Kadakia, K.; Park, S. K.; Kumta, P. N. Tin and Graphite Based Nanocomposites: Potential Anode for Sodium Ion Batteries. *J. Power Sources* **2013**, *225*, 316−322.

(8) Kim, Y.; Kim, Y.; Choi, A.; Woo, S.; Mok, D.; Choi, N. S.; Jung, Y. S.; Ryu, J. H.; Oh, S. M.; Lee, K. T. Tin Phosphide as a Promising Anode Material for Na-Ion Batteries. *Adv. Mater.* **2014**, *26*, 4139−4144.

(9) Dutta, P. K.; Sen, U. K.; Mitra, S. Excellent Electrochemical Performance of Tin Monosulphide (SnS) as a Sodium-Ion Battery Anode. *RSC Adv.* **2014**, *4*, 43155−43159.

(10) Song, J.; Yu, Z.; Gordin, M. L.; Hu, S.; Yi, R.; Tang, D.; Walter, T.; Regula, M.; Choi, D.; Li, X. Chemically Bonded Phosphorus/Graphene Hybrid as a High Performance Anode for Sodium-Ion Batteries. *Nano Lett.* **2014**, *14*, 6329−6335.

(11) Yu, D. Y. W.; Prikhodchenko, P. V.; Mason, C. W.; Batabyal, S. K.; Gun, J.; Sladkevich, S.; Medvedev, A. G.; Lev, O. High-Capacity Antimony Sulphide Nanoparticle-Decorated Graphene Composite as Anode for Sodium-Ion Batteries. *Nat. Commun.* **2013**, *4*, 2922.

(12) Fan, L.; Zhang, J.; Cui, J.; Zhu, Y.; Liang, J.; Wang, L.; Qian, Y. Electrochemical Performance of Rod-Like Sb-C Composite as Anodes for Li-Ion and Na-Ion Batteries. *J. Mater. Chem. A* **2015**, *3*, 3276−3280.

(13) Ko, Y. N.; Kang, Y. C. Electrochemical Properties of Ultrafine Sb Nanocrystals Embedded in Carbon Microspheres for Use as Na-Ion Battery Anode Materials. *Chem. Commun.* **2014**, *50*, 12322−12324.

(14) Wang, Z.; Qie, L.; Yuan, L.; Zhang, W.; Hu, X.; Huang, Y. Functionalized N-Doped Interconnected Carbon Nanofibers as an Anode Material for Sodium-Ion Storage With Excellent Performance. *Carbon* **2013**, *55*, 328−334.

(15) Ponrouch, A.; Goñi, A.; Palacín, M. R. High Capacity Hard Carbon Anodes for Sodium Ion Batteries in Additive Free Electrolyte. *Electrochem. Commun.* **2013**, *27*, 85−88.

(16) Wu, L.; Hu, X.; Qian, J.; Pei, F.; Wu, F.; Mao, R.; Ai, X.; Yang, H.; Cao, Y. Sb-C Nanofibers With Long Cycle Life as an Anode Material for High-Performance Sodium-Ion Batteries. *Energy Environ. Sci.* **2014**, *7*, 323−328.

(17) Su, D.; Wang, C.; Ahn, H.; Wang, G. Octahedral Tin Dioxide Nanocrystals as High Capacity Anode Materials for Na-Ion Batteries. *Phys. Chem. Chem. Phys.* **2013**, *15*, 12543−12550.

(18) Zhu, Y.; Han, X.; Xu, Y.; Liu, Y.; Zheng, S.; Xu, K.; Hu, L.; Wang, C. Electrospun Sb/C Fibers for a Stable and Fast Sodium-Ion Battery Anode. *ACS Nano* **2013**, *7*, 6378−6386.

(19) Xiao, L.; Cao, Y.; Xiao, J.; Wang, W.; Kovarik, L.; Nie, Z.; Liu, J. High Capacity, Reversible Alloying Reactions in SnSb/C Nanocomposites for Na-Ion Battery Applications. *Chem. Commun.* **2012**, *48*, 3321−3323.

(20) Wang, Y.; Su, D.; Wang, C.; Wang, G. SnO_2@MWCNT Nanocomposite as a High Capacity Anode Material for Sodium-Ion Batteries. *Electrochem. Commun.* **2013**, *29*, 8−11.

(21) Wang, Y.-X.; Lim, Y.-G.; Park, M.-S.; Chou, S.-L.; Kim, J. H.; Liu, H.-K.; Dou, S.-X.; Kim, Y.-J. Ultrafine SnO_2 Nanoparticle Loading Onto Reduced Graphene Oxide as Anodes for Sodium-Ion Batteries With Superior Rate and Cycling Performances. *J. Mater. Chem. A* **2014**, *2*, 529−534.

(22) Su, D.; Ahn, H.-J.; Wang, G. SnO_2@Ggraphene Nanocomposites as Anode Materials for Na-Ion Batteries With Superior Electrochemical Performance. *Chem. Commun.* **2013**, *49*, 3131−3133.

(23) Bonino, C. A.; Ji, L.; Lin, Z.; Toprakci, O.; Zhang, X.; Khan, S. A. Electrospun Carbon-Tin Oxide Composite Nanofibers for Use as Lithium Ion Battery Anodes. *ACS Appl. Mater. Interfaces* **2011**, *3*, 2534−2542.

(24) Dirican, M.; Yanilmaz, M.; Fu, K.; Lu, Y.; Kizil, H.; Zhang, X. Carbon-Enhanced Electrodeposited SnO_2/Carbon Nanofiber Composites as Anode for Lithium-Ion Batteries. *J. Power Sources* **2014**, *264*, 240−247.

DOI: 10.1021/acsami.5b04338
ACS Appl. Mater. Interfaces 2015, 7, 18387−18396

(25) Ji, L.; Lin, Z.; Guo, B.; Medford, A. J.; Zhang, X. Assembly of Carbon-SnO_2 Core-Sheath Composite Nanofibers for Superior Lithium Storage. *Chem. - Eur. J.* **2010**, *16*, 11543−11548.
(26) Lin, Z.; Ji, L.; Woodroof, M. D.; Zhang, X. Electrodeposited MnOx/Carbon Nanofiber Composites for Use as Anode Materials in Rechargeable Lithium-Ion batteries. *J. Power Sources* **2010**, *195*, 5025−5031.
(27) Wu, M.-S.; Ou, Y.-H.; Lin, Y.-P. Electrodeposition of Iron Oxide Nanorods on Carbon Nanofiber Scaffolds as an Anode Material for Lithium-Ion Batteries. *Electrochim. Acta* **2010**, *55*, 3240−3244.
(28) Li, Y.; Guo, B.; Ji, L.; Lin, Z.; Xu, G.; Liang, Y.; Zhang, S.; Toprakci, O.; Hu, Y.; Alcoutlabi, M.; Zhang, X. Structure Control and Performance Improvement of Carbon Nanofibers Containing a Dispersion of Silicon Nanoparticles for Energy Storage. *Carbon* **2013**, *51*, 185−194.
(29) Fu, K.; Xue, L.; Yildiz, O.; Li, S.; Lee, H.; Li, Y.; Xu, G.; Zhou, L.; Bradford, P. D.; Zhang, X. Effect of CVD Carbon Coatings on Si@ CNF Composite as Anode for Lithium-Ion Batteries. *Nano Energy* **2013**, *2*, 976−986.
(30) Rasheed, A.; Howe, J. Y.; Dadmun, M. D.; Britt, P. F. The Efficiency of the Oxidation of Carbon Nanofibers With Various Oxidizing Agents. *Carbon* **2007**, *45*, 1072−1080.
(31) Lin, Z.; Ji, L.; Zhang, X. Electrodeposition of Platinum Nanoparticles Onto Carbon Nanofibers for Electrocatalytic Oxidation of Methanol. *Mater. Lett.* **2009**, *63*, 2115−2118.
(32) Li, Y.; Lv, X.; Lu, J.; Li, J. Preparation of SnO_2-Nanocrystal/ Graphene-Nanosheets Composites and Their Lithium Storage Ability. *J. Phys. Chem. C* **2010**, *114*, 21770−21774.
(33) Chen, J. S.; Cheah, Y. L.; Chen, Y. T.; Jayaprakash, N.; Madhavi, S.; Yang, Y. H.; Lou, X. W. SnO_2 Nanoparticles With Controlled Carbon Nanocoating as High-Capacity Anode Materials for Lithium-Ion Batteries. *J. Phys. Chem. C* **2009**, *113*, 20504−20508.
(34) Ji, L.; Zhang, X. Electrospun Carbon Nanofibers Containing Silicon Particles as an Energy-Storage Medium. *Carbon* **2009**, *47*, 3219−3226.
(35) Liu, J.; Liu, H.; Yang, T.; Wang, G.; Tade, M. O. Mesoporous Carbon With Large Pores as Anode for Na-Ion Batteries. *Chin. Sci. Bull.* **2014**, *59*, 2186−2190.
(36) Fu, L.; Tang, K.; Song, K.; van Aken, P. A.; Yu, Y.; Maier, J. Nitrogen Doped Porous Carbon Fibres as Anode Materials for Sodium Ion Batteries With Excellent Rate Performance. *Nanoscale* **2014**, *6*, 1384−1389.
(37) Ji, L.; Gu, M.; Shao, Y.; Li, X.; Engelhard, M. H.; Arey, B. W.; Wang, W.; Nie, Z.; Xiao, J.; Wang, C. Controlling SEI Formation on SnSb-Porous Carbon Nanofibers for Improved Na Ion Storage. *Adv. Mater.* **2014**, *26*, 2901−2908.
(38) Jian, Z.; Zhao, L.; Pan, H.; Hu, Y.-S.; Li, H.; Chen, W.; Chen, L. Carbon Coated $Na_3V_2(PO_4)_3$ as Novel Electrode Material for Sodium Ion Batteries. *Electrochem. Commun.* **2012**, *14*, 86−89.

DOI: 10.1021/acsami.5b04338
ACS Appl. Mater. Interfaces 2015, 7, 18387−18396